Simultaneous 0.8, 1.0, and 1.3 μm multispectral and common-path broadband source for optical coherence tomography

Meng-Tsan Tsai[1] and Ming-Che Chan[2,3,*]

[1]*Department of Electrical Engineering, Chang Gung University, 259, School of Electrical and Computer Engineering, College of Engineering, Wen-Hwa 1st Road, Kwei-Shan, Tao-Yuan 33302, Taiwan*

[2]*Institute of Imaging and Biomedical Photonics, College of Photonics, National Chiao-Tung University, No. 301, Gaofa 3rd Rd., Guiren Dist., Tainan City 71150, Taiwan*

[3]*Department of Medical Research, Chi Mei Medical Center, Tainan 71004,Taiwan*

**Corresponding author: mcchan@nctu.edu.tw*

Received November 13, 2013; revised December 26, 2013; accepted December 28, 2013; posted January 2, 2014 (Doc. ID 201329); published February 6, 2014

Simultaneous multispectral generation in 0.8, 1.0, and 1.3 μm wavelength ranges by efficient energy conversions of 1.0 μm wavelength femtosecond pulses through a nonlinear fiber was reported. The output spectral range of this multispectral light source was composed of 0.6–0.9 μm blue-shifted Cherenkov radiation (CR), 1.0 μm residual pump, and 1.1–1.7 μm red-shifted soliton self-frequency shift (SSFS) with more than 1 mW/nm power-spectral densities. Output characteristics of the multispectral light source were then quantitatively analyzed and the central wavelengths of CR and SSFS emissions can be further easily adjusted by changing the input power into wavelength conversion fiber. Example spectral-domain optical coherence tomography (OCT) images of an IR card and finger skin were also performed with the demonstrated source. Due to the advantages of its simplicity, easily operated, and wavelength tunability, the reported multispectral source could be widely applicable for various spectroscopic OCT applications.

OCIS codes: (170.4500) Optical coherence tomography; (190.4370) Nonlinear optics, fibers; (300.6300) Spectroscopy, Fourier transforms.

http://dx.doi.org/10.1364/OL.39.000865

Optical coherence tomography (OCT) enables a 3D noninvasive biopsy of biological tissues by measuring the magnitude and echo time delay of back-scattered photons [1]. Recently, advanced by Fourier domain OCT (FD-OCT) including swept-source OCT (SS-OCT) [2–5] and spectral-domain OCT (SD-OCT) [6–10], the imaging speed has been greatly improved to hundred frames/s by the removal of mechanical scanning in the reference arm.

The previous reports have demonstrated that the spectroscopic properties of samples can be investigated by spectroscopic OCT [4–10]. Such spectroscopic information enables us to enhance the OCT image contrast, differentiate the different structures, and obtain wavelength-dependent parameters of biological tissues. With spectroscopic OCT, specific spectral features of a frog tadpole can be visualized [11]. Moreover, hemoglobin concentration and oxygen saturation levels can be estimated from spectroscopic OCT, which can be further utilized for cancer diagnosis [7,8]. Additionally, the lipid in atherosclerotic plaques can be identified with spectroscopic OCT [9]. Thus, spectroscopic OCT is capable of providing additional spectral features of biological samples for various applications.

However, the selection of operation wavelengths for studying the spectroscopic properties is a key issue. First, limited to the 0.7–1.3 μm optical window of most tissues and the development of light sources, the operated wavelengths for spectroscopic OCT were mainly focused on 0.8, 1.0, and 1.3 μm spectral ranges. Optic lights sources of 0.8 μm can provide better longitudinal resolutions. Light sources of 1.0 μm are most suitable for the applications in water-rich tissues because water absorption and dispersion in biological tissues are minimized in 1.0 μm spectral range. In contrast, the light sources in 1.3 μm spectral range can probe deeper tissue structures due to the lower scattering effect of bio-tissues [12]. Second, multispectral light sources are highly desired in FD-OCT because the higher wavelength-dependent absorption and scattering effect can be retrieved [4], and extracting the spectroscopic properties within one wavelength band is computationally expensive [5]. Finally, additional wavelength tuning capability to increase the separation in central wavelengths of the several wavelength bands is helpful to enhance the spectroscopic contrast [6,13].

In 2010, a multispectral *in vivo* 3D spectroscopic FD-OCT of human skin in 0.8, 1.0, and 1.3 μm regime was demonstrated with four different sources: a mode-locked Ti:sapphire laser, amplified spontaneous emissions, an ytterbium-doped fiber laser, and a superluminescence diode [10]. Systematic image comparisons of human skins, in terms of penetration depth, contrast, and resolution, were performed and additional contrasts for diagnosis and treatment monitoring in dermatology can be obtained.

However, fiber-based optical parametric amplification [4], multiple broadband sources [5,10], and complex filtered super-continuum source [6,13] were needed for multispectral spectroscopic investigation, which increases the system complexity and cost. Thus, according to the previous reports [6–10], the abovementioned broadband sources have demonstrated the ability of providing ultrahigh resolutions, but it is difficult to simultaneously emit multispectral ranges for investigation of spectroscopic properties of tissues, especially to cover

the three commonly used spectral ranges, 0.8, 1.0, and 1.3 μm, for OCT applications.

In this Letter, based on the Cherenkov radiation (CR) [14,15] and soliton self-frequency shift (SSFS) [16] effects of 1.0 μm femtosecond pulses inside a nonlinear photonic crystal fiber (PCF), we report a multispectral light source in 0.8, 1.0, and 1.3 μm wavelength ranges with a common path (single fiber) output. Femtosecond 1.0 μm laser pulses from excitation laser were simultaneously and efficiently wavelength blue-shifted and red-shifted to 0.6–0.9 and 1.1–1.7 μm regimes with more than 1 mW/nm power-spectral densities. The output characteristics of the multispectral OCT source were then quantitatively analyzed. Accordingly, the phenomenon was observed that central wavelengths of CR and SSFS emissions can be further easily adjusted by changing the input power inside the wavelength conversion fiber. Example SD-OCT images of an IR card and finger skin were also performed by the demonstrated multispectral light source.

Figure 1 shows the schematics of the proposed broadband multispectral source (shown in the dashed box) and the fiber-based SD-OCT system. The multispectral source was composed of a nonlinear PCF (SC-3.7-975, NKT Photonics) as a multispectral wavelength convertor and a 1030 nm miniaturized and air-cooled ytterbium femtosecond laser (Mikan, Amplitude Systems) as the excitation source. Typical average output power and fundamental repetition rate of the excitation laser were 1 W and 54.77 MHz respectively. The laser footprint was as small as 18×33 cm. Through the SSFS and CR processes inside the nonlinear fiber, the broadband 0.8, 1.0, and 1.3 μm multispectral emissions with high spectral density (above 1 mW/nm) were generated at the fiber exit. In this experiment, the launched power inside the nonlinear PCF was sequentially varied to tune the output wavelength of the output spectrum.

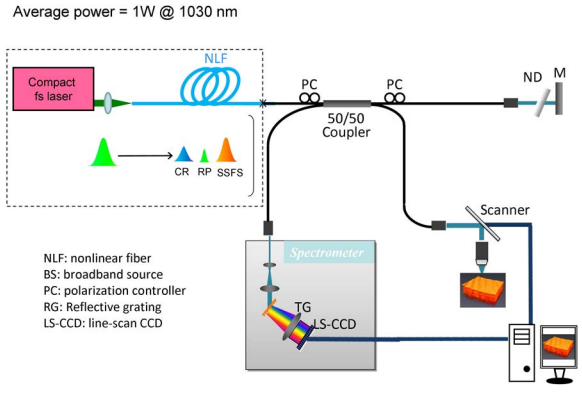

Fig. 1. Layout of the multispectral light source and related fiber-based SD-OCT system. Enclosed in the dashed box is the multispectral light source, whose output spectra are composed of three parts: blue-shifted Cherenkov radiation (CR), residual pump (RP), and red-shifted soliton self-frequency shift (SSFS). The remaining part shows the schematics of the related fiber-based spectral-domain OCT system. PCF, photonic crystal fiber; PC, polarization controller; ND, neutral density filter; TG, transmission grating; LS-CCD, line-scan charge-coupled device. The wavelength of the output spectrum can be tuned by varying the optical power in the PCF, the length of PCF, and the chirp of input pulse before PCF.

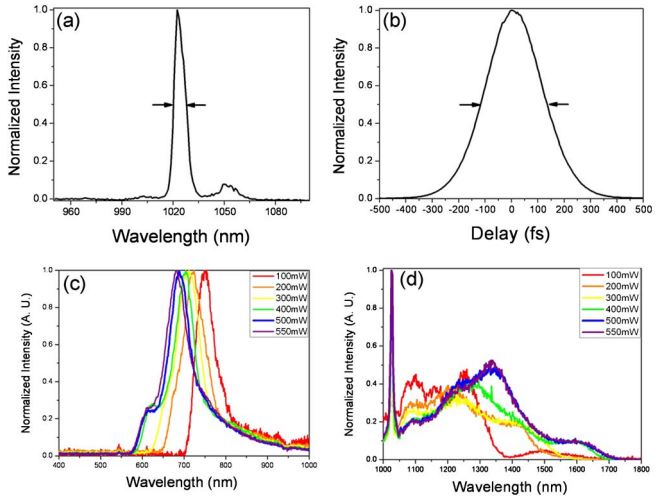

Fig. 2. (a) Output spectrum and (b) pulse-width measurement of the excitation 1030 nm laser. (c) Power-dependent spectra of the CR at fiber exit. (d) Power-dependent spectra of the RP and SSFS at fiber exit.

As shown in Figs. 2(a) and 2(b), the ytterbium laser emitted 250 fs pulses at a wavelength of 1.03 μm. The typical average output power and repetition rate of the 1.0 μm emissions were 1 W and 54.77 MHz, respectively. The output laser pulses were delivered into a 40 cm long nonlinear PCF with a typically 55% coupling efficiency. The wavelength of zero group-velocity dispersion of the nonlinear fiber was located at 975 nm and the dispersion value at 1030 nm was around 13 ps/nm/km. When 250 fs pulses at input wavelength of 1030 nm were launched into the PCF, due to high wavelength conversion efficiencies (>40%) from efficient CR and SSFS effect, high-power 0.8 μm CR and 1.3 μm SSFS emissions were realized in this experiment. We were able to couple a maximum total power of 550 mW (10 nJ pulse energy) into the nonlinear PCF. Figures 2(c) and 2(d) show CR, residual pump (RP), and SSFS spectra with different input powers into the nonlinear PCF.

For an OCT light source, the central wavelength, full-width half-maximum (FWHM) bandwidth, and optical power are the important parameters. The optical properties of light-tissue interactions are related to the spectral range of light source, determining the penetration depth and lateral resolutions [3,12]. The axial resolution is inversely proportional to FWHM of light source. Furthermore, the output power of light source in an OCT system is an important factor to determine the system sensitivity. Therefore, to further understand the output characteristics of a multispectral source for OCT applications, the relationships between the output power, central wavelength, FWHM, and pumping power were investigated. As shown in Fig. 3(a), according to the measured power-dependent CR, RP, and SSFS spectra, we quantitatively analyzed the central wavelength and FWHM. In Fig. 3(a), the blue, black, and red solid-lines show the central wavelength as a function of input power for CR, RP, and SSFS, respectively. Here, the central wavelengths of CR, RP, and SSFS emissions are defined as the mean value of short half-maximum wavelength and the long half-maximum wavelength. For the CR, the central

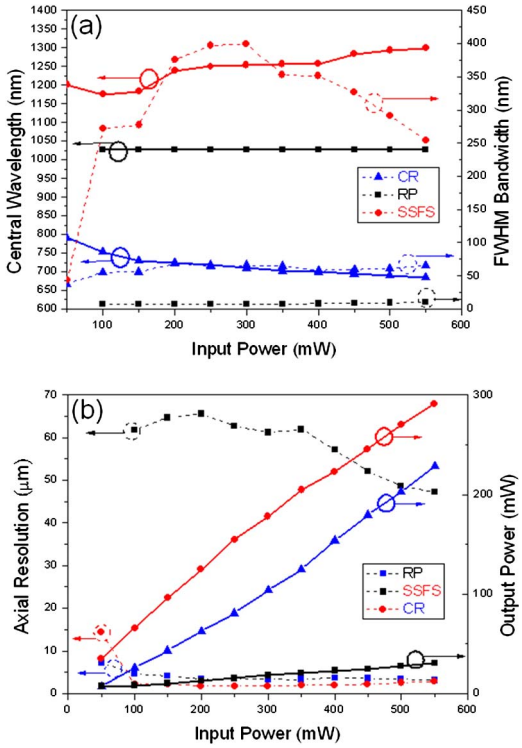

Fig. 3. Output characteristics of the multispectral light source. (a) Central wavelength (solid-lines) and FWHM bandwidth (dashed-lines) of CR (blue-triangle), RP (black-rectangular), and SSFS (red-circle) as the function of input power. (b) The output power (solid-lines) and corresponding axial resolution (dashed-lines) of CR (blue-triangle), RP (black-rectangular), and SSFS (red-circle) as the function of input power.

wavelength decreased from 792 to 684 nm as the input power increased from 50 to 550 mW. Central wavelengths of RP were always fixed within the 1026–1027 nm range at various input powers. Finally, the central wavelength of SSFS increased from 1201 to 1299 nm as the input power increased. According to the solid lines shown in Fig. 3(a), the central wavelength of SSFS and CR can be fine-tuned by simply controlling the coupling power inside the nonlinear PCF while the central wavelength of RP remain fixed at various input powers.

The FWHM bandwidth of an OCT light source is also a key factor because it is related to the axial resolution. Here, the FWHMs of CR, RP, and SSFS are defined as the difference between the long half-maximum wavelength and short half-maximum wavelength. As shown in Fig. 3(a), the blue, black, and red dashed-lines show the FWHMs as a function of input power for CR, RP, and SSFS, respectively. For the CR, with the increment of input power, CR bandwidths increased while the input power was below 200 mW and saturated while the input power was above 200 mW. For the RP, at various input powers, RP bandwidths slightly increased from 7 to 10 nm. Finally, the SSFS bandwidths increased when the input power was below 200 mW and decreased while the input power was above 200 mW.

According to the power-dependent central wavelengths and bandwidths of CR, RP, and SSFS, shown in Fig. 3(a), the theoretical axial resolutions of the CR, RP, and SSFS were calculated as shown in the colored dashed lines of Fig. 3(b). The theoretical axial resolution of OCT, Δz, which is related to the spectral range of the light source and the central wavelength of the light source, λ_0, can be expressed as $\Delta z \cong 0.44(\lambda_0^2/\Delta\lambda)$ [1]. The axial resolutions of CR and SSFS range from 3 to 5 μm and from 1 to 3 μm, respectively, when the input power inside nonlinear PCF was above 100 mW. The axial resolution of RP was on the order of tens of miliwatts, which was roughly the same as that of input 1030 nm femtosecond pulses.

Also, the output power of light source in an OCT system is an important factor to determine the system sensitivity. In Fig. 3(b), the solid lines show the output powers of CR, RP, and SSFS at different input powers. When the launched power inside the fiber was set to be 100 mW, the powers of CR, RP, and SSFS were 26, 8.3, and 65.7 mW, respectively. When the launched power inside the fiber was 150 mW, the powers of CR, RP, and SSFS became 43.4, 10.3, and 96.3, respectively. The power levels of the demonstrated multispectral sources at 0.8, 1.0, and 1.3 μm wavelength regions were sufficient for OCT imaging when the threshold launched power was as low as 100–150 mW inside fibers with a 250 fs pulse width. The power and pulse width requirements for a 1030 nm femtosecond light source can be addressed easily by currently available mode-locked lasers. For example, several groups demonstrated various compact and low-cost mode-locked fiber lasers, whose output power was above 150 mW and pulse width was below 250 fs [17,18].

At 550 mW launching power inside fiber, the optical power of the CR, residing in the 600–850 nm regimes, was ~229 mW with 41.6% power conversion efficiency. On the other hand, the SSFS residing in the 110–1600 bands, was with an output power of 291 mW, corresponding to 52.8% conversion efficiency. Finally, the RP was with a 30 mW, corresponding to a ~5.6% of total power. The calculated longitudinal resolutions of CR, RP, and SSFS are 3.14, 47.2, and 2.92 μm, respectively.

The central wavelength of CR and SSFS can be further expanded outside the 0.7–1.3 μm optical window by increasing the length of nonlinear fiber or replacing another nonlinear PCF with different dispersion and nonlinear properties [14]. Moreover, by varying the optical characteristics, such as the average power, polarization state, time width, and chirp, of input pulses, the central wavelength of SSFS and CR can be tuned easily [14]. The proposed multispectral light source can be further widely applied in other fields. On the other hand, the FWHM of CR and SSFS were broad-enough to provide an ultrahigh axial resolution for SD-OCT. The bandwidth of RP in this demonstration can also be improved by increasing the FWHM bandwidth of input pulses or using an extra nonlinear fiber.

To demonstrate the feasibility of a multispectral laser used as the OCT light source, the spectral range of induced CR was used as the light source in a SD-OCT system. As shown in Fig. 1, the multispectral light source was connected to an SD-OCT system, where the light was split into the reference and sample arms. In the reference arm, the collimated light was reflected by a reflection mirror. Two polarization controllers and a neutral density filter were inserted to adjust the optimal sensitivity. In contrast, the sample arm was composed of a two-axis

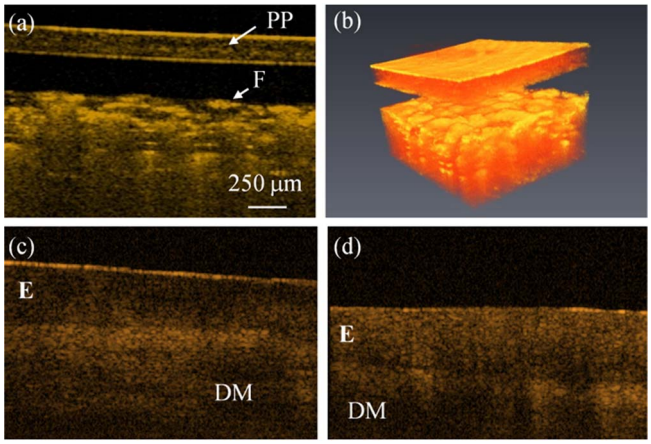

Fig. 4. (a) 2D- and (b) 3D-OCT result of IR card. (c) and (d) represent *in vivo* OCT results of fingertip and finger skin of one volunteer. PP, plastic plate; F, phosphor; E, epidermis; and DM, dermis.

galvanometer and a 10× objective lens, which can provide a transverse resolution of ~10 μm. Subsequently, the interference signal from the reference and sample arms was detected by a homemade spectrometer. In the spectrometer, the light from the collimator was expanded by a pair of achromatic lenses and then, diffracted by a reflective grating (GR50-1208, 1200 lp/mm, Thorlabs, New Jersey). Finally, the diffracted light was focused by an achromatic lens (AC508-150-B, Thorlabs, New Jersey) on a 2048 pixel line-scan camera (LSC) driven at a line rate of 25,000 lines/s (AViiVA EM1, e2 V, German) through a gigabit ethernet interface. Here, the spectrometer was only designed for a spectrum range of 730–870 nm, which can be used for the detection of CR. Although SD-OCT systems for 1.0 and 1.3 μm spectral regimes have not been demonstrated in this Letter, the SSFS and RP portions of multispectral emission can be detected by an InGaAs CCD-based spectrometer, which has been widely used for SD-OCT systems.

Figures 4(a) and 4(b) show 2D and 3D OCT results of the IR card, which consists of phosphors covered by the plastic plate. From the results, the plastic plate and particles of phosphors can be identified. Furthermore, Figs. 4(c) and 4(d) represent *in vivo* OCT results of fingertip and finger skin of one volunteer. The results show that the epidermis and dermis can be observed. Additionally, limited to the experimental facilities in 1.0 and 1.3 μm spectral regimes, only the SD-OCT system in 0.8 μm was demonstrated. However, one can see that such a multispectral light source enables application to spectroscopic OCT systems for investigation of spectroscopic properties of biological tissues.

In conclusion, based on the SSFS and CR effects inside a highly nonlinear PCF, a simple and easily operated multispectral broadband wavelength tunable source in the 0.8, 1.0, and 1.3 μm wavelength regime was reported. The induced 0.8 μm CR was connected to a SD-OCT system to demonstrate the feasibility. To develop a spectroscopic OCT system with the demonstrated source, a broadband fiber coupler can be used [19]. Moreover, to further reduce aberration and dispersion resulting from three spectral ranges in the sample arm, a reflective concave objective lens can be used, which is currently commercially available. Finally, three separate spectrometers are required for detection of 0.8, 1.0, and 1.3 μm interference spectrums. These demonstrated results show that such multispectral sources can provide a high resolution and a stable output for OCT applications. Thus, the demonstrated high-power broadband, multispectral light source able to perform wavelength tuning, which can be simply configured and easily operated, shows great potential for future multispectral FD-OCT applications such as biological research and industrial inspection.

The authors acknowledge the scientific discussions with Prof. C. K. Sun of National Taiwan University. This study was approved by the Chang Gung Medical Foundation Institutional Review Board (No. 101-2921A3) in Taiwan. This research was supported in part by the National Science Council of Taiwan, ROC (NSC 100-2221-E-009-092-MY3, NSC 102-2221-E-182 -061-MY2) and the Department of Medical Research of Chi-Mei Medical Center, Tainan.

References

1. D. Huang, E. A. Swanson, C. P. Lin, J. S. Schuman, W. G. Stinson, W. Chang, M. R. Hee, T. Flotte, K. Gregory, C. A. Puliafito, and J. G. Fujimoto, Science **254**, 1178 (1991).
2. R. Huber, M. Wojtkowski, and J. G. Fujimoto, Opt. Express **14**, 3225 (2006).
3. T.-H. Tsai, B. Potsaid, Y. K. Tao, V. Jayaraman, J. Jiang, P. J. S. Heim, M. F. Kraus, C. Zhou, J. Hornegger, H. Mashimo, A. E. Cable, and J. G. Fujimoto, Biomed. Opt. Express **4**, 1119 (2013).
4. R. Zhu, J. Xu, C. Zhang, A.-C. Chan, Q. Li, P. C. Chui, E. Y. Lam, and K. Wong, IEEE J. Sel. Top. Quantum Electron. **18**, 1287 (2012).
5. Y. Mao, S. Chang, E. Murdock, and C. Flueraru, Opt. Lett. **36**, 1990 (2011).
6. S. Kray, F. Spoler, M. Forst, and H. Kurz, Opt. Lett. **34**, 1970 (2009).
7. Y. Yasuno, Y. Hong, S. Makita, M. Yamanari, M. Akiba, M. Miura, and T. Yatagai, Opt. Express **15**, 6121 (2007).
8. J. Yi and X. Li, Opt. Lett. **35**, 2094 (2010).
9. C. P. Fleming, J. Eckert, E. F. Halpern, J. A. Gardecki, and G. J. Tearney, Biomed. Opt. Express **4**, 1269 (2013).
10. A. Alex, B. Povazay, B. Hofer, S. Popov, C. Glittenberg, S. Binder, and W. Drexler, J. Biomed. Opt. **15**, 026025 (2010).
11. U. Morgner, W. Drexler, F. X. Kärtner, X. D. Li, C. Pitris, E. P. Ippen, and J. G. Fujimoto, Opt. Lett. **25**, 111 (2000).
12. R. R. Anderson and J. A. Parrish, J. Invest. Dermatol. **77**, 13 (1981).
13. F. Spoler, S. Kray, P. Grychto, B. Hermes, J. Bornemann, M. Forst, and H. Kurz, Opt. Express **15**, 10832 (2007).
14. G. Q. Chang, L. J. Chen, and F. X. Kartner, Opt. Lett. **35**, 2361 (2010).
15. X. M. Liu, J. Lgsgaard, U. Moller, H. H. Tu, S. A. Boppart, and D. Turchinovich, Opt. Lett. **37**, 2769 (2012).
16. M. C. Chan, S. H. Chia, T. M. Liu, T. H. Tsai, M. C. Ho, A. A. Ivanov, A. M. Zheltikov, J. Y. Liu, H. L. Liu, and C.-K. Sun, IEEE Photon. Technol. Lett. **20**, 920 (2008).
17. H. W. Chen, J. K. Lim, S. W. Huang, D. N. Schimpf, F. X. Kartner, and G. Q. Chang, Opt. Express **20**, 28672 (2012).
18. K. Kieu, R. J. Jones, and N. Peyghambariab, Opt. Express **18**, 21350 (2010).
19. Y. Jung, G. Brambilla, and D. J. Richardson, Opt. Express **17**, 5273 (2009).